Land-use carbon emissions estimation for the Yangtze River Delta Urban Agglomeration using 1994-2016 Landsat image data

Cui, Yifan; Li, Long; Chen, Longqian; Zhang, Yu; Cheng, Liang; Zhou, Xisheng; Yang, Xiaoyan

Published in:
Remote Sensing

DOI:
10.3390/rs10091334

Publication date:
2018

License:
CC BY

Document Version:
Final published version

remote sensing

MDPI

Article

Land-Use Carbon Emissions Estimation for the Yangtze River Delta Urban Agglomeration Using 1994–2016 Landsat Image Data

Yifan Cui [1], Long Li [1,2], Longqian Chen [1,*], Yu Zhang [1,3], Liang Cheng [1,4], Xisheng Zhou [1], and Xiaoyan Yang [1,3]

[1] School of Environmental Science and Spatial Informatics, China University of Mining and Technology, Daxue Road 1, Xuzhou 221116, China; yifan.cui@cumt.edu.cn (Y.C.); long.li@cumt.edu.cn or long.li@vub.be (L.L.); yuzhang@cumt.edu.cn (Y.Z.); liang.cheng@cumt.edu.cn (L.C.); xisheng.zhou@cumt.edu.cn (X.Z.); xiaoyan.yang@jsnu.edu.cn (X.Y.)
[2] Department of Geography, Earth System Science, Vrije Universiteit Brussel, Pleinlaan 2, 1050 Brussels, Belgium
[3] School of Geography, Geomatics and Planning, Jiangsu Normal University, Shanghai Road 101, Xuzhou 221116, China
[4] Henry School of Agricultural Science and Engineering, Shaoguan University, Daxue Road 26, Shaoguan 512005, China
* Correspondence: chenlq@cumt.edu.cn; Tel.: +86-516-8359-1327

Received: 7 July 2018; Accepted: 20 August 2018; Published: 21 August 2018

Abstract: The amount and growth rate of carbon emissions have been accelerated on a global scale since the industrial revolution (1800), especially in recent decades. This has resulted in a significant influence on the natural environment and human societies. Therefore, carbon emission reduction receives continuously increasing public attention and has long been under debate. In this study, we made use of the land-use specific carbon emission coefficients from previous studies and estimated the land-use carbon emissions and carbon intensities of the Yangtze River Delta Urban Agglomeration (YRDUA)—which consists of 26 eastern Chinese cities—from Landsat image data and socio-economic statistics in 1995, 2005, and 2015. In addition, spatial autocorrelation models including both global and local Moran's I were used to analyze the spatial autocorrelation of carbon emissions and carbon intensities. It was found that (1) the YRDUA witnessed a rapidly increasing trend for net carbon emissions and a decreasing trend for carbon intensity over the two decades; (2) the spatial differences in carbon intensity had gradually narrowed, but were large in carbon emissions and had gradually increased; and (3) the carbon emissions in 2005 and 2015 had significant spatial autocorrelations. We concluded that (1) from 1995 to 2015 in the YRDUA, carbon emissions were large for the cities along the Yangtze River and carbon intensities were high for Anhui province's resource-based cities, while both carbon emissions and carbon intensities were small for Zhejiang province's cities; (2) over two decades, the increase in carbon emissions from urban land was approximately twice the increase in urban land area. Our study can provide useful insights into the assignment of carbon reduction tasks within the YRDUA.

Keywords: carbon dioxide; urban agglomeration; Yangtze River Delta; Landsat; land-use; spatial autocorrelation

1. Introduction

Carbon dioxide (CO_2) plays an important role in climate change, and its impact on climate change could be largely irreversible for 1000 years after carbon emissions stop [1]. Carbon emissions

are mainly from human activities including fossil-fuel burning and land-use change [2]. Compared with the burning of fossil fuel, there are more uncertainties in carbon emissions from land-use change [3–5]. Many studies have been carried out on carbon emissions from the land-use change on global, national, regional, and urban scales. These studies have provided us with land-use data and methods for estimating carbon emissions. For global carbon emissions estimation, national land-use statistics provided by FAO (Food and Agriculture Organization, Roman, Italy) [4,6], HYDE (History Database of the Global Environment) [3,7], and satellite data [4,8] are the main sources of land-use change information. Moreover, different models have been developed for carbon emissions estimation from historical land use, such as the bookkeeping model [9] and the terrestrial C-cycle model [3]. On the national scale, a variety of thematic maps, for example, of carbon density, vegetation, and soil type, were combined to calculate carbon emissions from land use [5]. Meanwhile, the IPCC (Intergovernmental Panel on Climate Change, Geneva, Switzerland) Guidelines for National Greenhouse Gas Inventories has provided a detailed carbon inventory and carbon coefficients [10] required for calculation. Satellite data remain to be used as an important land-use information source [5,11]. These IPCC methods are also widely applied to regional and urban carbon emissions estimation [12]. It is also noting that the capabilities of remote sensing to provide fine details and multi-temporal land-use information are highly appreciated at such scales [13,14].

As the world's second-largest economy as well as the largest carbon emitter [15,16], China should take and has already taken considerable responsibility for carbon reduction. At the Climate Change Paris Convention in Paris in November 2015, the Chinese government pledged to lower CO_2 emissions per unit GDP (gross domestic product) by 60% to 65% from the 2005 level by 2030 [5,17]. Most of the studies in China have focused mainly on the carbon emission characteristics of economically strong cities and provinces, such as Shanghai [18] and Jiangsu [12]. In order to properly distribute carbon emission reduction tasks to individual provinces, some studies [19–21] focus on the spatial heterogeneity of carbon emissions and carbon intensities in provinces and have concluded that northwestern and western provinces have high carbon emissions and carbon intensities, while southeastern regions usually have low carbon intensities.

However, these studies only investigated individual cities or provinces, but little considered how their carbon emissions were spatially correlated with their neighboring cities or provinces—which can provide important information on the spatial clustering characteristics of carbon emissions. The YRDUA lies in the intersection area of the "Belt and Road" and the "Yangtze River Economic Belt" and therefore plays a strategic role in the overall situation of modernization and the all-around opening structure of China [22,23]. What the spatiotemporal characteristics and spatial autocorrelations of carbon emissions and carbon intensities for important cities within large economic regions like the YRDUA are, is an important question that remains to be investigated.

In order to contribute to the general objective of providing insights into making carbon reduction policies and assigning carbon reduction tasks, this study monitors land-use carbon emissions and carbon intensities by means of satellite image data and socioeconomic statistics for the 26 cities of the YRDUA. Specific objectives are as follows: (1) to measure carbon emissions for carbon sources (which refer to land use types that emit carbon in the study) and carbon sinks (which refer to land use types that absorb carbon in the study) of the YRDUA in 1995, 2005, and 2015; (2) to characterize the spatiotemporal change of carbon emissions and carbon intensities in the 26 YRDUA cities, during 1995–2015; and (3) to examine the spatial autocorrelation of carbon emissions and carbon intensities using spatial correlation models and identify "hot" (high-high value) and "cold" (low-low value) cities in the YRDUA for different periods.

2. Study Area and Data

2.1. Study Area

As one of the most densely populated and economically significant regions in China, the Yangtze River Delta Urban Agglomeration (aka, the Yangtze River Delta Economic Zone) is located at the lower reach of the Yangtze River in eastern China (115°46′–123°25′E, 28°01′–34°28′N) and, according

to Chinese National Development and Reform Commission [24], consists of nine cities in Jiangsu Province; eight cities in Zhejiang Province; eight cities in Anhui Province; and Shanghai, which is a province-level municipality (Figure 1). It covers a geographical area of 211,700 km^2, approximately 2% of the whole of China's territory. In 2016, the 26 cities of the YRDUA produced a combined GDP of 14.87 trillion CNY (Chinese yuan) and accommodated a population of 152 million, which have reached approximately 19.99% and 10.97% of the entire country's GDP and population, respectively.

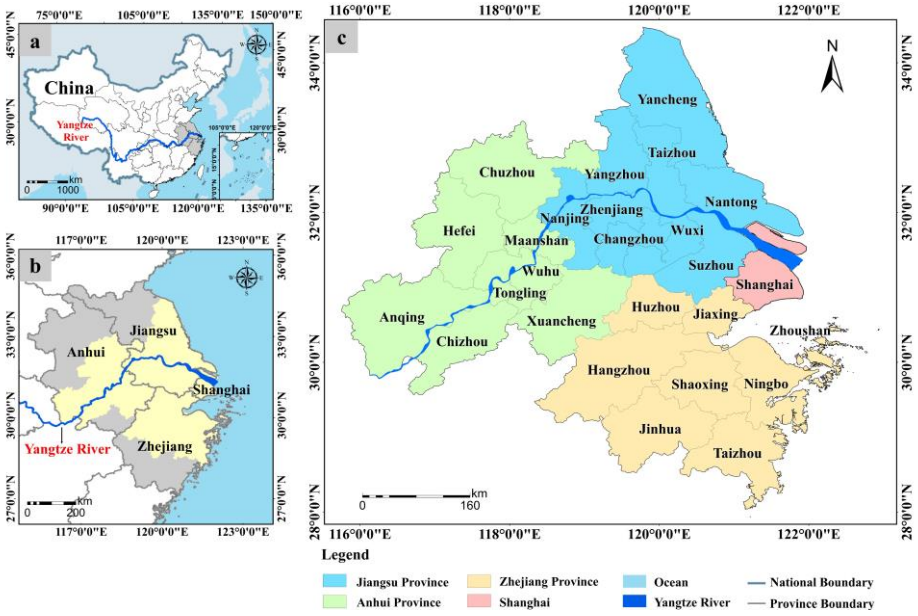

Figure 1. Study area. (**a**) The locations of Jiangsu, Zhejiang, Anhui provinces, Shanghai, and the Yangtze River in China; (**b**,**c**) the Yangtze River Delta Urban Agglomeration (YRDUA) consisting of 26 cities, eight of Jiangsu, nine of Zhejiang, eight of Anhui provinces, and the municipality of Shanghai.

2.2. Data

The data used in this study consist of remote sensing images and socio-economic statistics, which are raster-format and vector-format, respectively. To integrate the datasets for producing maps and spatial analyses, we then converted the classification images in raster format to a vector format.

2.2.1. Remote Sensing Images

Remote sensing images have proven powerful for monitoring land-use changes [13,14]. Landsat 5 TM (Thematic Mapper) and Landsat 8 OLI (Operational Land Imager) data were used in this study. The TM images consist of six spectral bands at a 30-m spatial resolution (bands 1–5 and 7), and one 120-m thermal band (band 6) [25]. The OLI images consist of nine spectral bands at a 30-m spatial resolution for bands 1 to 7 and 9, except for band 8, which is a panchromatic image at a spatial resolution of 15 m [26]. All remote sensing data were downloaded at no charge from the United States Geological Survey website (USGS, https://earthexplorer.usgs.gov/) (Table 1). Prior to image classification, we applied radiometric calibration, atmospheric correction (FLAASH), geo-referencing (image to image), and seamless mosaic (in which seamlines are automatically generated using seamline networks formed b area Voronoi diagrams with overlaps [27]) to these images. Afterward, we extracted the study area from the mosaicked images using vector data representing the administrative boundary of the YRDUA.

To understand the change in carbon emissions over time, a multi-temporal analysis was performed in this study. For a large geographical area like the YRDUA, we had to produce a mosaic image to cover the entire study area with 19 scenes. For each period, it is ideal if these 19 images were acquired in the same year and for the same months. This is, however, difficult for the YRDUA consisting of 26 large Chinese cities and almost impossible when considering image quality. As such,

we collected images acquired from 1994 to 1996, from 2004 to 2006, and from 2014 to 2016 for multi-temporal analysis. Nevertheless, we consider that annual variations were also limited in adjacent years and that seasonal variations were limited as these images were mainly acquired in warm months (i.e., May to September)—these months were approximately evenly distributed for each period. For the sake of simplicity, the 1994–1996, the 2004–2006, and the 2014–2016 periods were referred to as the years of 1995, 2005, and 2015 in this study.

Table 1. Landsat image data used in the study. TM—Thematic Mapper; OLI—Operational Land Imager.

Year	Sensor	Acquisition Date (Path/Row)
1995 (1994–1996)	TM	1994-05-05 (118/39), 1994-05-05 (118/40), 1994-05-19 (120/37), 1994-05-19 (120/39), 1994-05-19 (120/40), 1994-05-30 (117/40), 1994-06-29 (119/39), 1994-08-30 (121-39), 1995-06-05 (122/39), 1995-08-03 (119/37), 1995-08-03 (119/38), 1995-08-05 (117/39), 1995-08-12 (118/38), 1995-09-04 (119/40), 1995-09-02 (121/37), 1995-09-02 (121/38), 1995-10-13 (120/38), 1996-05-08 (120/36), 1996-07-25 (122/38)
2005 (2004–2006)	TM	2004-05-21 (121/39), 2004-07-19 (118/38), 2004-07-26 (119/39), 2004-07-26 (119/40), 2004-08-04 (118/40), 2004-09-17 (122/38), 2004-09-17 (122/39), 2005-05-12 (117/39), 2005-07-15 (117-40), 2006-04-20 (118/39), 2006-05-20 (120/37), 2006-05-20 (120/38), 2006-05-20 (120/39), 2006-07-30 (121/37), 2006-07-30 (121/38), 2006-09-09 (120/36), 2006-09-18 (119/37), 2006-09-18 (119/38), 2006-09-25 (120/40)
2015 (2014–2016)	OLI	2014-05-01 (121/39), 2014-05-26 (120/37), 2014-06-11 (120/39), 2015-05-13 (120/36), 2015-05-13 (120/40), 2015-07-27 (117/39), 2015-07-27 (117-40), 2015-08-03 (118/38), 2015-08-03 (118/39), 2015-08-03 (118/40), 2015-10-02 (122/39), 2015-10-13 (119/37), 2015-10-13 (119/38), 2015-10-13 (119/39), 2015-10-13 (119/40), 2016-04-29 (120/38), 2016-06-14 (122/38), 2016-07-25 (121/37), 2016-07-25 (121/38)

2.2.2. Socio-Economic Statistics

Energy consumption and GDP data are an important input for carbon emissions and carbon intensities estimation. They were collected for each of the 26 cities from their city-level and provincial statistical yearbooks. Figure 2 shows the general characteristics of the 26 YRDUA cities.

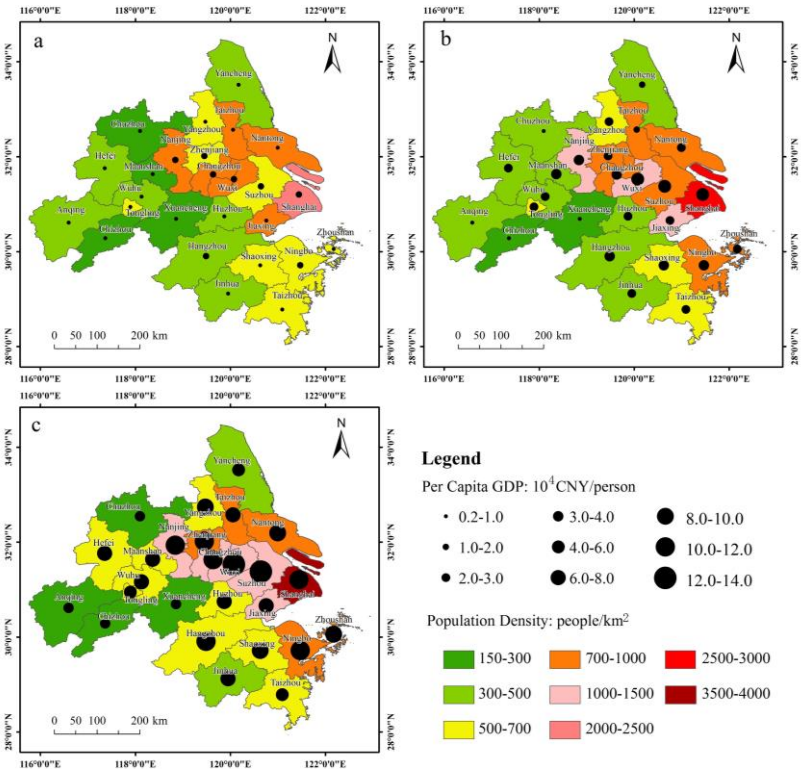

Figure 2. Population density and per capita gross domestic product (GDP) grading for the 26 YRDUA cities in 1995 (**a**), 2005 (**b**), and 2015 (**c**). The population here refers to the resident population.

Traditionally, each city annually reports its major types of energy consumption in its statistical yearbook, so these data are readily available. However, the statistics for each city showing their proportional uses of different fuel types are not detailed in the yearbooks, but they are not required in the study.

3. Methods

3.1. Land-Use Classification

3.1.1. Random Forest Classifier

In this study, random forests (RF) was considered for land cover/use mapping as it has been shown to provide good classification results [28,29]. It was performed in remote sensing image processing software package ENVI 5.1 Classic with a random forest classification add-in titled EnMAP-Box [30]. Random forest classification accuracy depends on the number of trees and the number of random features used for classification, which are two user-defined parameters [28,31]. Among the features were NDVI (Normalized Difference Vegetation Index) [32] and MNDWI (Modified Normalized Difference Water Area Index) [33], as they might improve classification accuracy. The OOB (out-of-bag) test was used to estimate the test set accuracy [28,29]. By trial and error, the number of trees and random vectors of 50 and 3, respectively, were considered best parameters used for random forest classification of land cover/use of the study area. Figure 3 shows the classification results.

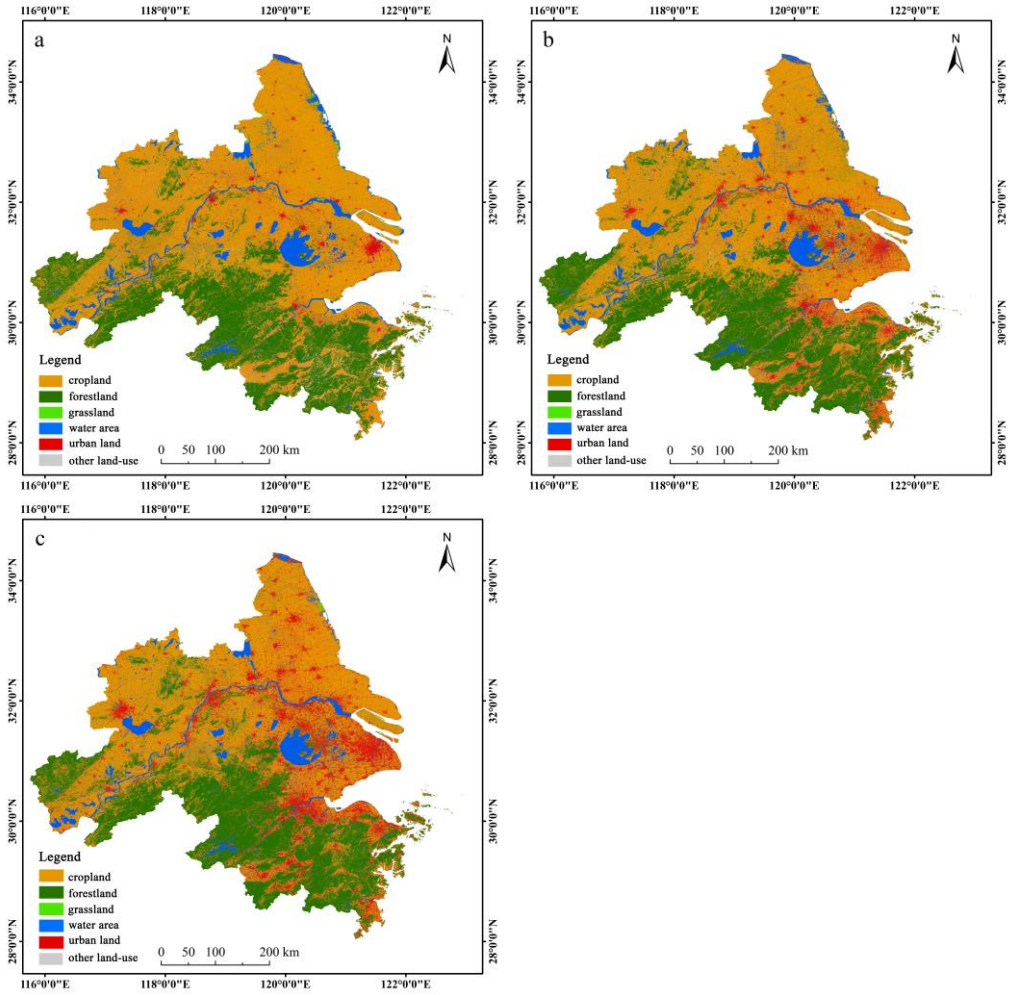

Figure 3. Land use classification maps of the YRDUA in 1995 (**a**), 2005 (**b**), and 2015 (**c**).

3.1.2. Accuracy Assessment

For a better land cover/use characterization of the study area, and thus a better carbon emissions estimation, we decided to classify the remote sensing images of the study area into six broad categories, namely, cropland (including fallow), forestland, grassland, water area, urban land, and other land-use. High-resolution satellite images in Google Earth Pro were used to assess classification accuracy for the 2014–2016 period. A total of 2000 sample points were first randomly generated in the classified image in 2015 with ArcGIS 10.2, and then were imported over the historic satellite images archived in Google Earth Pro for obtaining the ground-truthing data for the 2014–2016 period through visual image interpretation. A confusion matrix was constructed, and classification accuracy was calculated for each period by programming in MATLAB R2016a. The overall accuracy and the kappa coefficients were 88.60% and 0.8311, respectively, for the 2014–2016 period. The classification results were rather acceptable as the kappa coefficient is greater than 0.7 [34]. Because the historical satellite images in Google Earth Pro for the 1994–1996 and the 2004–2006 periods were also mainly 30-m resolution Landsat data, accuracy assessment based on them is incomparable to that based on high-resolution images. On the other hand, images of the three periods are the same type and are processed and classified using the same procedure and approach, we thus consider that similar classification accuracies were obtained for the 1994–1996 and 2004–2006 periods. As such, we did not conduct independent accuracy assessments for the two earlier periods.

3.2. Estimation of Carbon Emissions

3.2.1. Carbon Emissions from Land Use

This study only focuses on the carbon emissions caused by land-use changes and does not consider the effect of land-use management. Land-use carbon emissions can be estimated by the following equation:

$$E_i = \sum e_i = \sum S_i \times \delta_i \times \frac{M_{CO_2}}{M_C} \quad (1)$$

where E_i is the carbon emissions from land use; i refers to the type of land-use; S_i is the area of land i; and δ_i is the carbon emission coefficient for land i, whose positive values indicate carbon emission while negative values indicate carbon absorption; M_{CO_2}/M_C is the ratio of the mass carbon dioxide molecules to a carbon atom—44/12. Previous studies have proposed the coefficients for different land use types (Table 2). We use either the values directly or their means in this study. It is noted that the carbon emission coefficients of forestland and grassland are relatively small and the difference is large. This is because there is a large spatial difference in the carbon sink of vegetated land, especially grassland, in China.

Table 2. Carbon emission coefficients for the five land-use types classified from Landsat image data.

Land-Use Types	Carbon Emission Coefficient (kg (C)·m^{-2}·a^{-1})	Used in the Study
Cropland	0.0497 [35]	0.0497
Forestland	[−0.0645, −0.0527] [36]	−0.0586
Grassland	−0.0021 [36]	−0.0021
Water area	−0.0509 [37] −0.0410 [38]	−0.0459
Other land-use	−0.0005 [38]	−0.0005

3.2.2. Carbon Emissions from Energy Consumption

Energy consumption is generally assumed to occur only in factories in urban land. Therefore, we attributed carbon emissions to urban land. In this study, nine types of fuel were considered, including coal, cleaned coal, coke, gasoline, kerosene, diesel oil, fuel oil, liquefied petroleum gas, and natural gas. Their carbon emissions can be calculated using the following equation [10]:

$$E_C = \sum E_{ci} \times f_i \times \frac{M_{CO_2}}{M_C} \quad (2)$$

$$f_i = A_i \times B_i \times C_i \quad (3)$$

where E_c is the total carbon emissions from energy consumption; E_{ci} is the amount of consumption of fuel i; f_i is the carbon emission coefficient for fuel i; M_{CO_2}/M_C is the ratio of the mass carbon dioxide molecules to a carbon atom—44/12; and A_i, B_i, and C_i are the average low calorific value, the unit calorific value carbon content, and the carbon oxidation rate of fuel, respectively (Table 3). The average low calorific values and carbon oxidation rates were obtained from the guidelines for the preparation of provincial greenhouse gas inventories of China [39]. The guidelines were prepared by the China Energy Research Institute, Tsinghua University, and the Institute of Atmospheric Sciences of the Chinese Academy of Science, among others, according to the situation in China. It provides default values of the parameters of different fuel types that are used in the absence of locally measured data. The unit calorific value carbon contents were obtained from the China Energy Statistic Yearbook 2016 [40].

Table 3. Values of the parameters required for estimating carbon emissions from energy consumption.

Energy	Average Low Calorific Value (kJ/kg)	Unit Calorific Value Carbon Content (kg/10^9 J)	Carbon Oxidation Rate (%)	Carbon Emission Coefficient (kg/kg)
Coal	20,908	26.37	94	
Cleaned coal	26,344	25.41	93	0.6225
Coke	28,435	29.5	93	0.7801
Gasoline	43,070	18.9	98	0.7977
Kerosene	43,070	19.5	98	0.8231
Diesel oil	42,652	20.2	98	0.8443
Fuel oil	41,816	21.1	98	0.8647
Liquefied petroleum gas	50,179	17.2	98	0.8458
Natural gas	35,585	15.3	99	0.5390

3.2.3. Carbon Intensity

Carbon intensity is the carbon emissions from per unit of GDP, which is given as follows:

$$CI = \frac{CE}{GDP} \quad (4)$$

where CI is the carbon emission intensity; CE is the total carbon emissions; and GDP is the gross domestic product of a given area. The carbon intensity in this study refers to the carbon intensity of energy consumption.

3.3. Spatial Autocorrelation Model

Spatial autocorrelation refers to the degree of spatial correlation between an attribute value of a spatial unit and the same attribute value of a neighboring spatial unit, and can characterize the agglomeration characteristics of spatial unit attributes [41,42]. Both global and local spatial autocorrelation models were used in this study.

3.3.1. Global Spatial Autocorrelation Model

Global Moran's I is the most commonly used test statistic for describing spatial autocorrelation in the univariate map or in regression residuals [41]. In the study, it was used to describe the degree of spatial association and significance. It is given by the following equation [43]:

$$I = \frac{n\sum_{i=1}^{n}\sum_{j=1}^{n} W_{ij}\left(\left(y_i - \overline{y}\right)\left(y_j - \overline{y}\right)\right)}{\sum_{i=1}^{n}\sum_{j=1}^{n} W_{ij}\sum_{i=1}^{n}\left(y_j - \overline{y}\right)^2}\left(i \neq j\right) \quad (5)$$

where y_i is the variable of region i (I = 1, 2, 3, ..., n); $\overline{y}$ is the average value of all regions; y_j is the variable of other regions (where $j \neq i$); and W_{ij} is the spatial weight matrix (when region i and region j are topologically adjacent with a common edge, $W_{ij} = 1$, otherwise $W_{ij} = 0$).

Moran's I ranges between −1 and 1. A positive Moran's I value indicates a positive spatial autocorrelation, while a negative Moran' I value indicates a negative spatial autocorrelation. When Moran's I = 0, the variable obeys the stochastic spatial distribution [43,44]. The larger the absolute value, the stronger the spatial autocorrelation, and vice versa.

The normalized statistics z(I) of the Moran's I approximately obey the normal distribution [43]:

$$z(I) = \frac{I - E(I)}{\sqrt{Var(I)}} \sim N(0,1) \quad (6)$$

where Var(I) is the theoretical variance of the Moran's I; $E(I) = -1/(n-1)$ is the mean.

3.3.2. Local Spatial Autocorrelation Model

Local Moran's I is a local indicator of spatial autocorrelation. It is widely used to identify "hot spots" and "cold spots" in the entire area and to classify them into the spatial cluster and spatial outliners [42,44,45]. It is given as follows [44]:

$$I_i = \frac{\left(y_i - \overline{y}\right)}{\sigma^2}\sum_{j=1,j\neq i}^{n}\left[W_{ij}\left(y_j - \overline{y}\right)\right] \quad (7)$$

where y_i is the variable of region i (i = 1, 2, 3..., n); y_j is the variable of other regions (where $j \neq i$); $\overline{y}$ is the average value of all regions; σ^2 is the variance of y; and W_{ij} is the weight matrix normalized by the row (sum of each row is 1).

A region with a positive local Moran's I value indicates that it has the similar values to its neighbors and the regions are called spatial clusters. In contrast, a negative value indicates the region has different values from its neighbors and the regions are called spatial outliers. Spatial clusters include high-high clusters (high value around is high) and low-low clusters (low value around in value), spatial outliers include high-low clusters (high value is low around) and low-high clusters (low value is high around) [44]. The results of all regions are shown in Moran scatter plots, while only regions that passed the significance test are shown in LISA (Local Indicators of Spatial Association) cluster maps. A Moran scatter plots has four quadrants, which are labeled as high-high (HH), low-low (LL), high-low (HL), and low-high (LH). All regions are scattered in these four quadrants based on their local Moran's I index. Consistent with the Moran scatter plot, there are four types of regions in the LISA cluster map including high-high, low-low, high-low, and low-high regions, as well as high-high regions and low-low regions, also known as "hot spots" and "cold spots", respectively [44].

In this study, local Moran's I was used to identify the "hot" cities (hot spots) and "cold" cities (cold spots) from the YRDUA, based on 999 permutations at the significance level of 5%. Meanwhile, the Moran's I and z(I) were calculated in ArcGIS 10.2, and Moran scatter plots and LISA cluster maps were drawn in GeoDa 1.12.

4. Results

4.1. Land Use and Carbon Emissions of the YRDUA

Land use of the YRDUA in 1995, 2005, and 2015 and changes over the two decades are shown in Table 4. There was a rapid increase in urban land and a significant decrease in cropland over the two decades. By contrast, little change was observed for forestland, grassland, water area, and other land-use.

Table 4. Areas and proportions of six land-use types in the Yangtze River Delta Urban Agglomeration (YRDUA) in 1995, 2005, and 2015. Change rates refer to the ratio of their area change during 1995–2015 to the original area in 1995.

Year	Unit	Cropland	Forestland	Grassland	Water Area	Urban Land	Other Land-Use
1995	area (km^2)	121,871.6	58,240.1	1338.3	14,949.5	9100.7	3953.4
	proportion	58.19%	27.81%	0.64%	7.14%	4.33%	1.89%
2005	area(km^2)	115,285.4	61,710.4	1092.0	14,642.3	14,626.8	2096.9
	proportion	55.04%	29.46%	0.51%	6.99%	6.98%	1.00%
2015	area(km^2)	105,485.7	61,242.7	1234.1	13,801.0	25,175.9	2514.2
	proportion	50.36%	29.24%	0.59%	6.59%	12.02%	1.20%
1995–2015	area of change	−16,385.9	3002.6	−104.2	−1148.5	16,075.1	−1439.2
	change rate	−13.45%	5.16%	−7.78%	−7.68%	176.64%	−36.40%

Based on the land use data given in Table 4, land-use specific carbon emissions and absorptions, the total carbon emissions and absorptions, and the net carbon emissions (which is the total carbon emissions minus the total carbon absorptions) (Table 5) were estimated with Equation (1).

Negative figures correspond to carbon sinks, for example, for forestland, grassland, water area, and other land-use, while positive figures correspond to carbon sources, for example, for cropland and urban land (Table 5). It is noticeable that forestland and urban land were the largest contributors to carbon absorptions and carbon emissions, respectively. The carbon absorptions of forestland accounted for more than 83% of the total carbon absorptions for each period and increased from 1251.39 × 10^4 t to 1315.93 × 10^4 t over the two decades. Regarding urban land, its carbon emissions were 111,578.4 × 10^4t (accounted for approximately 98% of the total emissions) in 2015, which was four times more than that in 1995. Carbon emissions from per unit urban land increased from 26.57 $kg \cdot m^{-2} \cdot a^{-1}$ to 44.32 $kg \cdot m^{-2} \cdot a^{-1}$, and the average annual growth was 0.8875 $kg \cdot m^{-2}$.

Overall, the two decades saw a rapid increase in the net carbon emissions, by approximately four times (87,055.8 × 10^4 t), from 24,895.3 × 10^4 t in 1995 to 111,951.1 × 10^4 t in 2015, with an average annual rise of 17.5%. Carbon absorptions showed only a 44.9 × 10^4 t increase, which was, however, dwarfed by the increase in carbon emissions.

Table 5. The land-use specific carbon emissions and absorptions, the total carbon emissions and absorptions, and the net carbon emissions of the YRDUA for different periods (unit: 10^4 t). Percentages for cropland and urban land refer to their contribution to the net carbon emissions, while percentages for forestland, grassland, water area, and other land-use refer to their contribution to the carbon absorptions.

Year	Land-Use Specific Carbon Emission/Absorptions						Total Carbon Emissions	Total Carbon Absorptions	Net Carbon Emissions
	Cropland	Forestland	Grassland	Water Area	Urban Land	Other Land-Use			
1995	2220.9	−1251.4	−1.0	−251.6	24,179.1	−0.7	26,400.0	−1504.7	24,895.3
	8.41%	83.16%	0.07%	16.72%	91.59%	0.05%	100.00%	100.00%	
2005	2100.9	−1326.0	−0.8	−246.4	70,728.8	−0.4	72,829.7	−1573.6	71,256.1
	2.88%	84.26%	0.05%	15.66%	97.12%	0.02%	100.00%	100.00%	
2015	1922.3	−1316.0	−0.9	−232.3	111,578.4	−0.5	113,500.7	−1549.6	111,951.1
	1.69%	84.92%	0.06%	14.99%	98.31%	0.03%	100.00%	100.00%	

4.2. Spatiotemporal Characteristics of Carbon Emissions

4.2.1. Temporal Characteristics

Figure 4 shows the land-use specific carbon emissions (CE) and carbon absorptions (CA) of the 26 cities in 1995, 2005, and 2015. Carbon absorptions were shown to be steady, while carbon emissions saw contrasting increases for the 26 cities. Over the two decades, large increases in carbon emissions were observed for Shanghai, Suzhou, Nanjing, Ningbo, and Maanshan, while very few were observed for Chuzhou, Xuancheng, Chizhou, and Anqing.

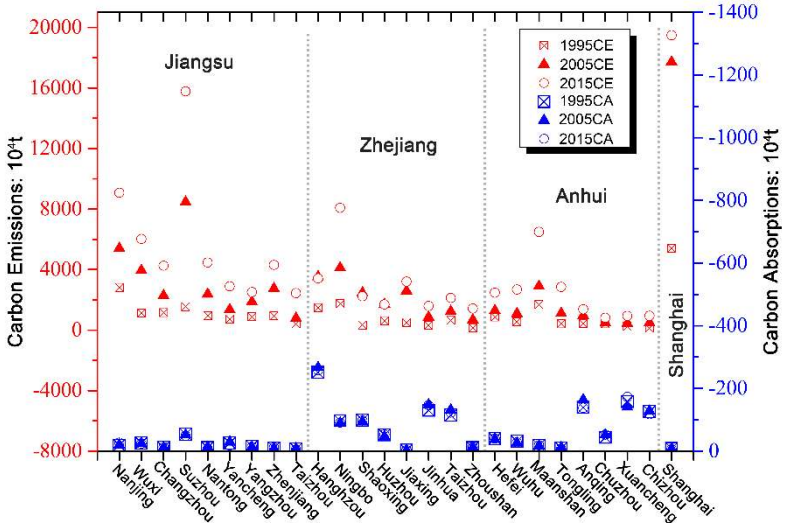

Figure 4. Land-use specific carbon emissions (CE) and carbon absorptions (CA) of the 26 YRDUA cities in 1995, 2005, and 2015.

Figure 5 presents the annual net carbon emissions (ANCE) during the first (1995–2005) and second (2005–2015) decades, respectively. For most Jiangsu cities, their net carbon emissions tended to increase steadily, and their ANCE changes were smaller in the first decade than in the second decade. Hangzhou, Shaoxing, Huzhou, and Jiaxing in Zhejiang Province had equivalent net carbon emissions in 2005 and 2015, with drastic drops in their annual average net carbon emissions. Small NCE changes were observed for all the eight Anhui cities, while significant increases in annual average net carbon emissions were shown only for Maanshan, Tongling, Wuhu, and Hefei. Regarding Shanghai, its net carbon emissions increased steadily in the second decade after an obvious rise in the first decade.

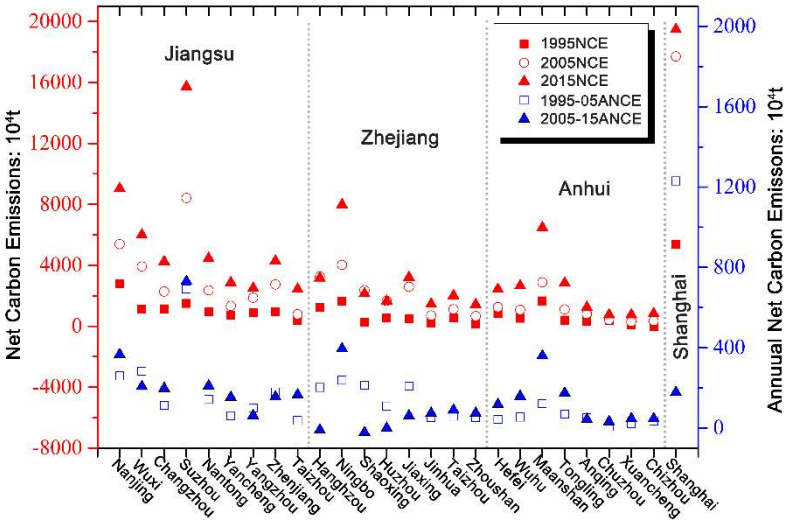

Figure 5. Land-use specific net carbon emissions (NCE) and annual net carbon emissions (ANCE) for the 26 YRDUA cities in 1995, 2005, and 2015.

Figure 6 shows a decreasing trend in the carbon intensities for all the YRDUA cities over the two decades. In addition, the gap between the carbon intensities of cities gradually narrowed. The average carbon intensity for the YRDUA dropped from 2.2791 t/10^4 Yuan to 0.8234 t/10^4 Yuan. The carbon intensities decreased significantly for Maanshan, Tongling, Hefei, and Wuhu, while it appeared to increase and then decreased for Suzhou, Shaoxing, Jiaxing, Zhoushan, and Chizhou.

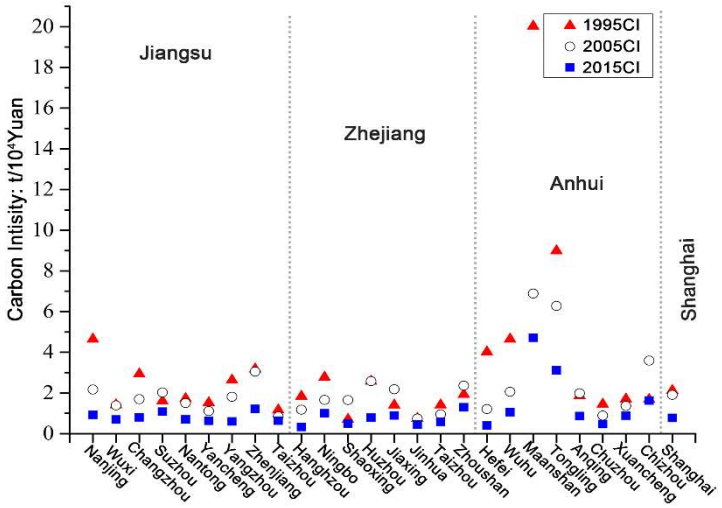

Figure 6. Carbon intensities (CI) for the 26 YRDUA cities from 1995 to 2015.

4.2.2. The Spatial Characteristics

Based on net carbon emissions and carbon intensities, the 26 YRDUA cities were classified into different levels, respectively (Figure 7).

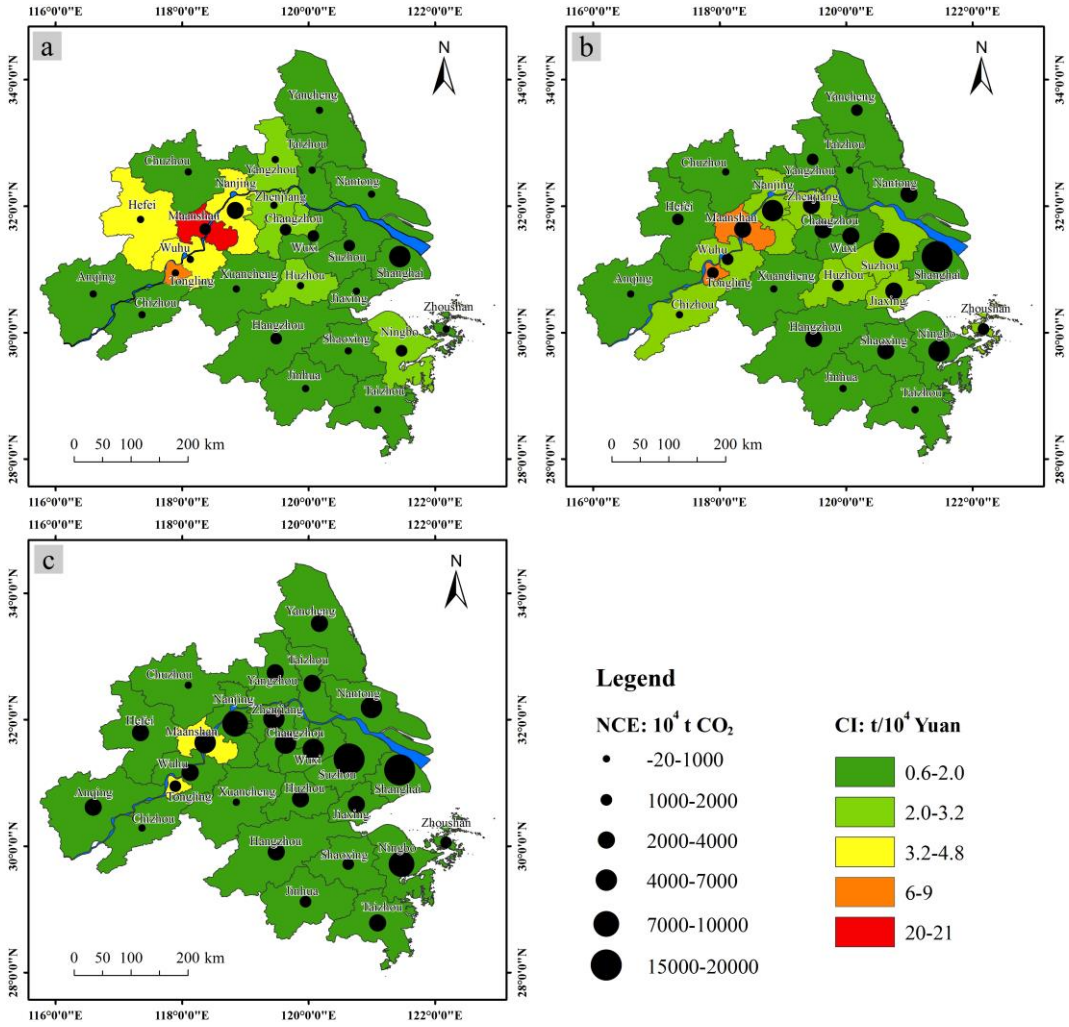

Figure 7. Net carbon emissions (NCE) and carbon intensities (CI) grading for the 26 YRDUA cities in 1995 (**a**), 2005 (**b**), and 2015 (**c**).

Despite a large difference in net carbon emissions among these cities, we noticed that along the Yangtze River, there were gradual increases, from Tongling to Wuhu, to Maanshan, and to Nanjing in the west YRDUA, and from Zhenjiang, to Changzhou, to Wuxi, to Suzhou, and to Shanghai in the east YRDUA, respectively. Shanghai always had the highest NCE, immediately followed by Suzhou and then by Wuxi in 2005 and 2015, except for in 1995. Over the two decades, the highest NCE in the west YRDUA was observed for Nanjing, followed by Maanshan and then by Wuhu.

Carbon intensity of the YRDUA, however, showed contrasting spatial distribution over the three periods (Figure 7). For example, despite the highest net carbon emissions, Shanghai had a relatively low carbon intensity. Highest carbon intensities were observed for Maanshan and Tongling, both in Anhui. Higher intensities were mostly located in the west YRDUA in 1995, but were only in Maanshan and Tongling in 2015. Except for Maanshan and Tongling, carbon intensities were generally low in the YRDUA, all below 1.5.

4.3. Spatial Correlation of Carbon Emissions and Carbon Intensity

4.3.1. Global Spatial Autocorrelation

The Global Moran's I and z(I) of net carbon emissions and carbon intensities were calculated in ArcGIS10.2 (Table 6). In order to include Zhoushan for the analysis, Zhoushan and Ningbo were set adjacent when calculating the spatial weight matrix.

There was significant positive spatial autocorrelation in the net carbon emissions of the YRDUA in 2005 and 2015 as the Moran's I values were positive and the z(I) was greater than 1.96 for the two periods. Regarding carbon intensity, although all the Moran's I values for the three periods were positive, none were significant.

Table 6. The global Moran's I and z(I) of carbon emissions and carbon intensities of the YRDUA in 1995, 2005, and 2015.

	Net Carbon Emissions			**Carbon Intensities**		
Year	**1995**	**2005**	**2015**	**1995**	**2005**	**2015**
Moran's I	−0.0012	0.1984	0.1910	0.0729	0.0412	0.0056
z(I) *	0.3894	2.6056	2.0116	1.3937	0.7064	0.4574

* z(I) > 1.96 indicates significance at the 5% level, and z(I) > 2.58 indicates significance at the 1% level.

4.3.2. Local Spatial Autocorrelation

As the global Moran's I values of net carbon emissions in 2005 and 2015 passed the significance test, we drew the Moran scatter plots of net carbon emissions for two periods (Figure 8). The number of cities in the HH and LL quadrants was fourteen and fifteen, accounting for 54% and 58% of the total (26 cities) in 2005 and 2015, respectively, indicating that spatial homogeneity and local accumulation pattern of net carbon emissions were significant.

In addition, the LISA cluster maps (Figure 9) were also produced to show the type of the cities that passed the significance test. From Figure 9, it was observed that (1) Shanghai and Suzhou (Figure 9b,c) had a relatively high degree of stability in the "hot" cities of net carbon emissions from 2005 to 2015; (2) the "cold" cities of net carbon emissions (Figure 9a–c) varied greatly—they decreased in number and shifted to the southeast over the two decades; and (3) the significant "cold" cities of carbon intensity were located in Zhejiang province, while Wuhu remained a significant "hot" city in 20 years (Figure 9d–f). According to Figure 2, the per capita GDP and population density of Shanghai and Suzhou were similar and large in 2005 and 2015. Also, Wuxi, Nantong, and Jiaxing, which are adjacent to Shanghai and Suzhou, have a relatively high population density. This may result in both adjacent cities being "hot" cities of net carbon emissions in 2005 and 2015, as the impact of population and economy on carbon emissions is positive.

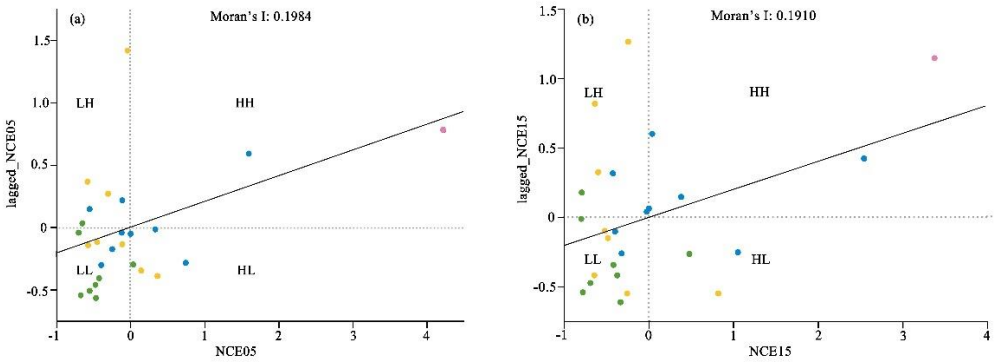

Figure 8. Moran scatter plots of net carbon emissions for the YRDUA in 2005 (**a**) and 2015 (**b**). Green, blue, yellow, and rose represent the cities of Anhui, Jiangsu, and Zhejiang provinces, and Shanghai, respectively. H—high; L—low.

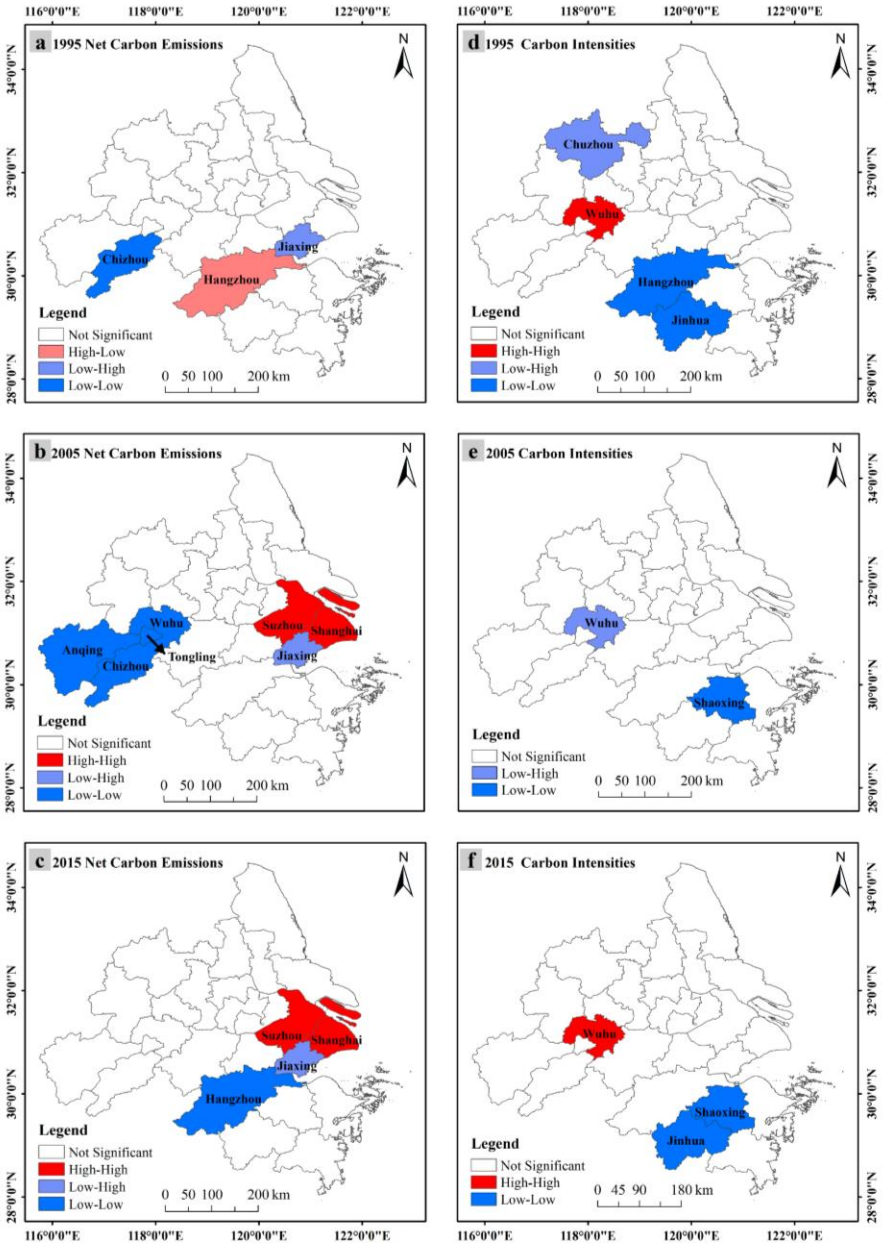

Figure 9. LISA cluster maps of net carbon emissions (**a**–**c**) and carbon intensities (**d**–**f**) for the YRDUA in 1995, 2005, and 2015.

5. Interpretation and Discussion

In our study, we obtained land use information from multi-temporal Landsat images by applying random forest classification and estimated land-use specific carbon emissions for the YRDUA in 1995, 2005, and 2015. In addition, the spatial correlation of net carbon emissions and carbon intensities were also calculated. In this section, we interpreted the results and discussed their implications.

5.1. Carbon Sources and Carbon Sinks

Multi-temporal land cover/use mapping illustrated a rapid increase in urban land and a significant decrease in cropland in the YRDUA over the entire study period (Table 4). The was because, since the beginning of the 1990s, the entire Yangtze River Delta (YRD) has entered an era of rapid economic development [46]. It was characterized by unprecedented industrialization and urbanization, resulting in growing cities and towns, and continuous conversion from cropland into urban land [47,48]. As such, carbon emissions from urban land increased accordingly (Table 4). It is noted that urban land changed 177.6%, while carbon emissions changed 361.5%, which is much larger than the increase of urban land. We can conclude that the increase of area is not the main reason for the increase in carbon emissions from urban land. We considered that the main reason is the growing population. Figure 2 shows an increasing trend in the population density for most of the YRDUA cities over the two decades. The impact of population on carbon emissions is mainly reflected in two aspects: on the one hand, the increase in population leads to rising demand for food, clothing, housing, and transportation service, which has promoted production; on the other hand, overconsumption and waste become increasingly remarkable in China as human consumption habits change.

Urban land was responsible for most of the carbon emissions in the YRDUA, which is consistent with previous studies [12,49]. Its contribution to carbon emissions increased from 91.6% to 98.3% from 1995 to 2015 (Table 5). Although forestland can absorb carbon dioxide, its area made little gains during the two decades (Table 4). This suggests that the increase in carbon emissions from urban land was far greater than the increase in carbon absorption by forestland. The ratio of carbon emissions from urban land to carbon absorption by forestland rose from 19.3 in 1995 to 84.8 in 2015.

Therefore, carbon emission reduction should be focused on controlling carbon emissions from urban land and maintain, if not expand, forestland and grassland. The key to reducing carbon emissions from urban land is optimizing land-use management and structure. It has been proven that land-use structure and land-use management have a positive influence on carbon emission reduction in China [5,12]. Still, as the largest populated developing country in the world, China is however not determined to reduce carbon emissions too much at the cost of slowing down its economic growth.

5.2. Characteristics of Carbon Emissions and Carbon Intensity

In summary, from the perspective of the YRDUA, Shanghai and cities along the Yangtze River had high carbon emissions (Figure 7). Cities in Anhui had high carbon intensity particularly in 1995 and 2005 (Figure 6), mainly because of its slow economic development, inappropriate industrial structure, energy consumption structure, and large primary energy consumption [50]. Statistics show that its secondary industry proportion of Anhui has exceeded 50% and that its energy consumption has been traditionally dominated by coal and oil. In China, secondary industries proportion and primary energy consumption usually tend to strengthen carbon intensity [50,51]. Located in central China, Anhui has been traditionally neglected by the central government in terms of regional development strategy. Until 2014, it was officially included in the Yangtze River Delta. It was no surprise that its economic development lagged and will continue to lag behind its coastal neighbors such as Jiangsu, Zhejiang, and Shanghai.

Net carbon emissions in Shanghai rose significantly from 1994 to 2016 (Figure 5)—due mainly to its prosperous Pudong New District, which was established in 1990 and later recognized as a national strategic position in 1992 [52,53]. Pudong New District has since promoted the rapid

economic development of Shanghai in the following decades. Shanghai's proportion of China's GDP rose from 4.08% in 1995 to 4.92% in 2005—this process went with increased energy consumption and carbon emissions [50,54].

It is interesting that the highest carbon intensities were observed for Maanshan and Tongling, much larger than those for the other 24 cities, particularly in 1995 (Figure 7). This could be explained by the fact that both Maanshan and Tongling are typical mineral resource-based cities. The economic accumulation of resource-based cities is mainly based on the exploitation of large quantities of raw resources [55]. Resource-based cities in China are usually characterized by a heavy economic dependency on the exploitation and consumption of large quantities of raw resources [55]. Maanshan and Tongling have large iron and copper reserves, respectively, and there are many factories related to steel, foundry, machinery, and so on. In earlier decades, low efficiency and a waste of resources were serious in these industries due to technological limitations and carbon intensities of the two cities being high in the 1990s.

Based on the results and analysis, the carbon emissions of Shanghai, Nanjing, Suzhou, Wuxi, and Changzhou along the Yangtze River should be strictly controlled. Regarding cities in Anhui province, it is necessary to accelerate the optimization and upgrading of their industrial structures, and thus to promote technological innovation in carbon emission reduction [16,56].

5.3. Spatial Autocorrelation of Carbon Emissions and Carbon Intensity

Values of net carbon emissions for the YRUDA in 2005 and 2015 were shown to have significant spatial autocorrelations. From the Moran scatter plots (Figure 8), we observed that Moran scatters were mainly focused on the LL quadrant, which is consistent with the grading of net carbon commission (Figure 7). The net carbon emissions from the north, west, and south of the YRDUA were all lower and there were more cities with the lowest level carbon emissions. Both indicate that in the YRDUA, the low-value cluster was obvious in 2005 and 2015.

Shanghai and Suzhou were significant "hot" cities (Figure 9b,c), mainly because of rapid economic development. It has been proven that economic growth accelerates carbon emissions in China [51]. The decreasing number and shift to the southeast of "cold" cities (Figure 9a–c) were because traditional high-energy-consuming industries had gradually been relocated from eastern coastal regions to central and western provinces. This also explains why Hangzhou changed from a high-low city in 1995 to a low-low city in 2015. In 1995, there was no "hot" city (Figure 9a). Cities with the largest carbon emissions were Shanghai, immediately followed by Nanjing, and then by Ningbo and Maanshan. They were scattered, thus there was no high-value cluster.

Zhejiang province was found to have the most "cold" cities (Figure 9d–f) in terms of carbon intensity, because Zhejiang had already made an effort to adjust and upgrade its industrial structure, pursuing an economic structure decreasingly dependent on energy, but driven by knowledge innovation and capital intensiveness. In the first decade, Wuhu was a significant "hot" city (Figure 9d,f) in terms of carbon intensity because Wuhu is adjacent to high carbon intensity cities, particularly Maanshan and Tongling. We hope that this finding may help the provincial and local governments of Anhui raise general awareness of their high carbon intensities.

5.4. Limitations

Although this study has improved the accuracy of land cover/use mapping by performing robust random forest classification on Landsat remote sensing image data, and although it used the carbon emission coefficients applicable for the Chinese context, caution should be taken in over-interpreting our results: (1) because of data acquisition limitations, only energy consumption of industries was considered for estimating carbon emissions from urban land—this means that we might underestimate the carbon emissions for the YRDUA, and that the underestimate might be 5–10% [18,57,58]; (2) carbon emission coefficients for cropland, forestland, grassland, water area, and other land use were acquired from multiple studies where these coefficients were determined using a variety of methods. More work is needed to verify or improve these coefficients.

6. Conclusions

To provide carbon emission characteristics for policymakers to formulate carbon emission reduction policies, this study focuses on remote sensing-based carbon emissions estimation for the Yangtze River Delta Urban Agglomeration over two decades from 1995 to 2015. In addition, both global and local Moran's I statistics were used to analyze the spatial autocorrelations of net carbon emissions and carbon intensities. The key findings and main conclusions are summarized as follows:

- In the YRDUA, urban land contributed to almost all carbon emissions. Furthermore, total carbon emissions and per unit of carbon emissions from urban land increased rapidly over twenty years. Thus, carbon emission reduction should be focused on controlling carbon emissions from urban land.
- There were high carbon emissions for cities along the Yangtze River and high carbon intensities for cities in Anhui. Therefore, the carbon emissions of Shanghai and other cities along the Yangtze River should be strictly controlled. Regarding cities in Anhui province, it is necessary to accelerate the optimization and upgrading of their industrial structures to low carbon intensity.
- Carbon intensities of Maanshan and Tongling, known as resource-based cities, were much higher than those of the other 24 cities. The government of Anhui Province should pay more attention to the economic development model and carbon intensities of resourced-based cities.

In summary, carbon emissions from urban land should be strictly controlled, especially for cities along the Yangtze River, and industrial structure and energy structure of Anhui province need to be optimized to improve the low-carbon economy. Our study will contribute to decision-makers to develop carbon emission reduction policies for the YRDUA.

Author Contributions: Y.C. and L.L. contributed equally to the study. They conceived the study through discussion with L.C. (Longqian Chen). They conducted image analysis and result interpretation and wrote the manuscript. Y.Z. and X.Z. contributed to data collection and pre-processing, and L.C. (Liang Cheng) and X.Y. advised in the discussion section. L.C. (Longqian Chen) supervised the study and finalized the paper. All the authors reviewed and approved the final manuscript version.

Funding: This research was funded by the Fundamental Research Funds for the Central Universities under grant number 2018ZDPY07.

Acknowledgments: The authors thank the United States Geological Survey (USGS) for providing the Landsat data freely. Furthermore, we appreciate the editors and reviewers for their constructive comments and suggestions.

Conflicts of Interest: The authors declare no conflict of interest.

References

1. Solomon, S.D.; Plattner, G.-K.; Knutti, R.; Friedlingstein, P. Irreversible climate change due to carbon dioxide emissions. *Proc. Natl. Acad. Sci. USA* **2009**, *106*, 1704–1709, doi:10.1073/pnas.0812721106.
2. Le Quéré, C.; Raupach, M.R.; Canadell, J.G.; Marland, G.; Bopp, L.; Ciais, P.; Conway, T.J.; Doney, S.C.; Feely, R.A.; Foster, P.; et al. Trends in the sources and sinks of carbon dioxide. *Nat. Geosci.* **2009**, *2*, 831–836, doi:10.1038/ngeo689.
3. Van Minnen, J.G.; Goldewijk, K.K.; Stehfest, E.; Eickhout, B.; van Drecht, G.; Leemans, R. The importance of three centuries of land-use change for the global and regional terrestrial carbon cycle. *Clim. Chang.* **2009**, *97*, 123–144, doi:10.1007/s10584-009-9596-0.
4. Houghton, R.A.; House, J.I.; Pongratz, J.; Van Der Werf, G.R.; Defries, R.S.; Hansen, M.C.; Le Quéré, C.; Ramankutty, N. Carbon emissions from land use and land-cover change. *Biogeosciences* **2012**, *9*, 5125–5142, doi:10.5194/bg-9-5125-2012.
5. Lai, L.; Huang, X.; Yang, H.; Chuai, X.; Zhang, M.; Zhong, T.; Chen, Z.; Chen, Y.; Wang, X.; Thompson, J.R. Carbon emissions from land-use change and management in China between 1990 and 2010. *Sci. Adv.* **2016**, *2*, 1–8, doi:10.1126/sciadv.1601063.
6. Ramankutty, N.; Foley, J.A. Estimating historical changes in global land cover: Croplands from 1700 to

1992. *Glob. Biogeochem. Cycles* **1999**, *13*, 997–1027, doi:10.1029/1999GB900046.
7. Goldewijk, K.K. Estimating global land use change over the past 300 years: The HYDE Database. *Glob. Biogeochem. Cycles* **2001**, *15*, 417–433, doi:10.1029/1999gb001232.
8. Defries, R.S.; Houghton, R.A.; Hansen, M.C.; Field, C.B.; Skole, D.; Townshend, J. Carbon emissions from tropical deforestation and regrowth based on satellite observations for the 1980s and 1990s. *Proc. Natl. Acad. Sci. USA* **2002**, *99*, 14256–14261, doi:10.1073/pnas.182560099.
9. Houghton, R.A. The annual net flux of carbon to the atmosphere from changes in land use 1850–1990*. *Tellus* **2004**, *51B*, 378–390, doi:10.1034/j.1600-0889.1999.00013.x.
10. IPCC. Carbon emission factor. In *2006 IPCC Guidelines for National Greenhouse Gas Inventories*, 1st ed.; Eggleston, H.S., Buendia, L., Eds.; Institute for Global Environmental Strategies: Hayama, Japan, 2006; p. 23, ISBN 92-9169-520-3.
11. Castillo-Santiago, M.A.; Hellier, A.; Tipper, R.; de Jong, B.H.J. Carbon emissions from land-use change: An analysis of causal factors in Chiapas, Mexico. *Mitig. Adapt. Strateg. Glob. Chang.* **2007**, 1213–1235, doi:10.1007/s11027-006-9060-7.
12. Chuai, X.; Huang, X.; Wang, W.; Zhao, R.; Zhang, M.; Wu, C. Land use, total carbon emissions change and low carbon land management in Coastal Jiangsu, China. *J. Clean. Prod.* **2015**, *103*, 77–86, doi:10.1016/j.jclepro.2014.03.046.
13. Muttitanon, W.; Tripathi, N.K. Land use/land cover changes in the coastal zone of Ban Don Bay, Thailand using Landsat 5 TM data. *Int. J. Remote Sens.* **2005**, *26*, 2311–2323, doi:10.1080/0143116051233132666.
14. Rogan, J.; Chen, D.M. Remote sensing technology for mapping and monitoring land-cover and land-use change. *Prog. Plan.* **2004**, *61*, 301–325, doi:10.1016/S0305-9006(03)00066-7.
15. Mu, H.; Li, H.; Zhang, M.; Li, M. Analysis of China's carbon dioxide flow for 2008. *Energy Policy* **2013**, *54*, 320–326, doi:10.1016/j.enpol.2012.11.043.
16. Guan, D.; Klasen, S.; Hubacek, K.; Feng, K.; Liu, Z.; He, K.; Geng, Y.; Zhang, Q. Determinants of stagnating carbon intensity in China. *Nat. Clim. Chang.* **2014**, *4*, 1017–1023, doi:10.1038/nclimate2388.
17. China-U.S. Joint Presidential Statement on Climate Change. Available online: http://en.ndrc.gov.cn/newsrelease/201509/t20150929_755626 (accessed on 24 March 2018).
18. Wang, Y.; Ma, W.; Tu, W.; Zhao, Q.; Yu, Q. A study on carbon emissions in Shanghai 2000–2008, China. *Environ. Sci. Policy* **2013**, *27*, 151–161, doi:10.1016/j.envsci.2012.12.005.
19. Geng, Y.; Tian, M.; Zhu, Q.; Zhang, J.; Peng, C. Quantification of provincial-level carbon emissions from energy consumption in China. *Renew. Sustain. Energy Rev.* **2011**, *15*, 3658–3668, doi:10.1016/j.rser.2011.07.005.
20. Zhao, Y.; Nielsen, C.P.; McElroy, M.B. China's CO_2 emissions estimated from the bottom up: Recent trends, spatial distributions, and quantification of uncertainties. *Atmos. Environ.* **2012**, *59*, 214–223, doi:10.1016/j.atmosenv.2012.05.027.
21. Shan, Y.; Liu, J.; Liu, Z.; Xu, X.; Shao, S.; Wang, P.; Guan, D. New provincial CO_2 emission inventories in China based on apparent energy consumption data and updated emission factors. *Appl. Energy* **2016**, *184*, 742–750, doi:10.1016/j.apenergy.2016.03.073.
22. Zhang, M.; Xiao, H.; Sun, D.; Li, Y. Spatial differences in and influences upon the sustainable development level of the Yangtze River Delta Urban Agglomeration in China. *Sustainability* **2018**, *10*, 411, doi:10.3390/su10020411.
23. Ouyang, X.; Gao, B.; Du, K.; Du, G. Industrial sectors' energy rebound effect: An empirical study of Yangtze River Delta urban agglomeration. *Energy* **2018**, *145*, 408–416, doi:10.1016/j.energy.2018.01.009.
24. National Development and Reform Commission Housing and Urban-Rural Development Department Notice on Issuing the Development Plan of the Yangtze River Delta Urban Agglomeration. Available online: http://www.ndrc.gov.cn/zcfb/zcfbghwb/201606/t20160603_806390 (accessed on 24 March 2018). (In Chinese)
25. Chander, G.; Helder, D.L.; Markham, B.L.; Dewald, J.D.; Kaita, E.; Thome, K.J.; Micijevic, E.; Ruggles, T.A. Landsat-5 TM reflective-band absolute radiometric calibration. *IEEE Trans. Geosci. Remote Sens.* **2004**, *42*, 2747–2760, doi:10.1109/TGRS.2004.836388.
26. Zhang, Y.; Chen, L.; Wang, Y.; Chen, L.; Yao, F.; Wu, P.; Wang, B.; Li, Y.; Zhou, T.; Zhang, T. Research on the contribution of urban land surface moisture to the alleviation effect of urban land surface heat based on Landsat 8 data. *Remote Sens.* **2015**, *7*, 10737–10762, doi:10.3390/rs70810737.
27. Pan, J.; Wang, M.; Li, D.; Li, J. Automatic generation of seamline network using area voronoi diagrams with

overlap. *IEEE Trans. Geosci. Remote Sens.* **2009**, *47*, 1737–1744, doi:10.1109/TGRS.2008.2009880.
28. Li, L.; Solana, C.; Canters, F.; Kervyn, M. Testing random forest classification for identifying lava flows and mapping age groups on a single Landsat 8 image. *J. Volcanol. Geotherm. Res.* **2017**, *345*, 109–124, doi:10.1016/j.jvolgeores.2017.07.014.
29. Cutler, D.R.; Edwards, T.C.; Beard, K.H.; Cutler, A.; Hess, K.T.; Gibson, J.; Lawler, J.J. Random forests for classification in ecology. *Ecology* **2007**, *88*, 2783–2792, doi:10.1890/07-0539.1.
30. Waske, B.; van der Linden, S.; Oldenburg, C.; Jakimow, B.; Rabe, A.; Hostert, P. imageR-A user-oriented implementation for remote sensing image analysis with Random Forests. *Environ. Model. Softw.* **2012**, *35*, 192–193, doi:10.1016/j.envsoft.2012.01.014.
31. Gislason, P.O.; Benediktsson, J.A.; Sveinsson, J.R. Random forests for land cover classification. *Pattern Recognit. Lett.* **2006**, *27*, 294–300, doi:10.1016/j.patrec.2005.08.011.
32. Macarof, P.; Statescu, F. Comparasion of NDBI and NDVI as indicators of surface urban heat island effect in Landsat 8 imagery: A case study of Iasi. *Present Environ. Sustain. Dev.* **2017**, *11*, doi:10.1515/pesd-2017-0032.
33. Wang, Y.; Huang, F.; Wei, Y. Water body extraction from Landsat ETM+ image using MNDWI and K-T transformation. *Int. Conf. Geoinform.* **2013**, doi:10.1109/Geoinformatics.2013.6626162.
34. Janssen, L.L.F.; van der Wel, F.J.M. Accuracy assessment of satellite derived land-cover data: A review. *Photogramm. Eng. Remote Sens.* **1994**, *60*, 419–426.
35. Shi, H.; Mu, X.; Zhang, Y.; Lv, M. Effects of different land use patterns of carbon emisson in Guangyuan city of Sichuan province. *Bull. Soil Water Conserv.* **2012**, *32*, 101–106. (In Chinese)
36. Fang, J.Y.; Guo, Z.D.; Piao, S.L.; Chen, A.P. Terrestrial vegetation carbon sinks in China, 1981–2000. *Sci. China Ser. D Earth Sci.* **2007**, *50*, 1341–1350, doi:10.1007/s11430-007-0049-1.
37. Duan, X.; Wang, X.; Lu, F.; Ouyang, Z. Carbon sequestration and its potential by wetland ecosystems in China. *Acta Ecol. Sin.* **2008**, *28*, 463–469. (In Chinese)
38. Lai, L. Carbon Emission Effect of Land Use in China. Ph.D. Thesis, Nanjing University, Nanjing, Jiangsu, China, 2010. (In Chinese)
39. Guidelines for the Preparation of Provincial Greenhouse Gas Inventories of China. Available online: https://wenku.baidu.com/view/7ae95325f111f18583 (accessed on 30 March 2018). (In Chinese)
40. National Bureau of Statistics. *China Energy Statistical Yearbook 2016*, 1st ed.; China Stastistics Press: Beijing, China, 2016; pp. 356–358, ISBN 978-7-5037-8064-6. (In Chinese)
41. Tiefelsdorf, M. The saddlepoint approximation of Moran's I's and local Moran's Ii's reference sistributions and their numerical evaluation. *Geogr. Anal.* **2002**, *34*, 187–206, doi:10.1111/j.1538-4632.2002.tb01084.x.
42. Fu, W.J.; Jiang, P.K.; Zhou, G.M.; Zhao, K.L. Using Moran's i and GIS to study the spatial pattern of forest litter carbon density in a subtropical region of southeastern China. *Biogeosciences* **2014**, *11*, 2401–2409, doi:10.5194/bg-11-2401-2014.
43. Zhang, T.; Lin, G. On Moran's i coefficient under heterogeneity. *Comput. Stat. Data Anal.* **2016**, *95*, 83–94, doi:10.1016/j.csda.2015.09.010.
44. Zhang, C.; Luo, L.; Xu, W.; Ledwith, V. Use of local Moran's I and GIS to identify pollution hotspots of Pb in urban soils of Galway, Ireland. *Sci. Total Environ.* **2008**, *398*, 212–221, doi:10.1016/j.scitotenv.2008.03.011.
45. Yuan, Y.; Cave, M.; Zhang, C. Using local Moran's I to identify contamination hotspots of rare earth elements in urban soils of London. *Appl. Geochem.* **2018**, *88*, 167–178, doi:10.1016/j.apgeochem.2017.07.011.
46. Tian, G.; Jiang, J.; Yang, Z.; Zhang, Y. The urban growth, size distribution and spatio-temporal dynamic pattern of the Yangtze River Delta megalopolitan region, China. *Ecol. Model.* **2011**, *222*, 865–878, doi:10.1016/j.ecolmodel.2010.09.036.
47. Long, H.; Tang, G.; Li, X.; Heilig, G.K. Socio-economic driving forces of land-use change in Kunshan, the Yangtze River Delta economic area of China. *J. Environ. Manag.* **2007**, *83*, 351–364, doi:10.1016/j.jenvman.2006.04.003.
48. Deng, X.; Huang, J.; Rozelle, S.; Uchida, E. Growth, population and industrialization, and urban land expansion of China. *J. Urban Econ.* **2008**, *63*, 96–115, doi:10.1016/j.jue.2006.12.006.
49. Han, J.; Meng, X.; Zhou, X.; Yi, B.; Liu, M.; Xiang, W.-N. A long-term analysis of urbanization process, landscape change, and carbon sources and sinks: A case study in China's Yangtze River Delta region. *J. Clean. Prod.* **2017**, *141*, 1040–1050, doi:10.1016/j.jclepro.2016.09.177.
50. Wang, S.; Zhou, C.; Li, G.; Feng, K. CO_2, economic growth, and energy consumption in China's provinces: Investigating the spatiotemporal and econometric characteristics of China's CO_2 emissions. *Ecol. Indic.* **2016**,

69, 184–195, doi:10.1016/j.ecolind.2016.04.022.
51. Fan, Y.; Liu, L.C.; Wu, G.; Tsai, H.T.; Wei, Y.M. Changes in carbon intensity in China: Empirical findings from 1980–2003. *Ecol. Econ.* **2007**, *62*, 683–691, doi:10.1016/j.ecolecon.2006.08.016.
52. Marton, A.M.; Wu, W. Spaces of globalisation: Institutional reforms and spatial economic development in the Pudong new area, Shanghai. *Habitat Int.* **2006**, *30*, 213–229, doi:10.1016/j.habitatint.2004.02.004.
53. Wu, J.; Barnes, T. Local planning and global implementation: Foreign investment and urban development of Pudong, Shanghai. *Habitat Int.* **2008**, *32*, 364–374, doi:10.1016/j.habitatint.2007.11.003.
54. Hu, C.; Huang, X. Characteristics of carbon emission in China and analysis on its cause. *China Popul. Resour. Environ.* **2008**, *18*, 38–42, doi:10.1016/S1872-583X(09)60006-1.
55. He, S.Y.; Lee, J.; Zhou, T.; Wu, D. Shrinking cities and resource-based economy: The economic restructuring in China's mining cities. *Cities* **2017**, *60*, 75–83, doi:10.1016/j.cities.2016.07.009.
56. Wang, Z.; Zhang, B.; Liu, T. Empirical analysis on the factors influencing national and regional carbon intensity in China. *Renew. Sustain. Energy Rev.* **2016**, *55*, 34–42, doi:10.1016/j.rser.2015.10.077.
57. Cai, B.; Cao, D.; Liu, L.; Zhou, Y.; Zhang, Z. China transport CO_2 emission study. *Adv. Chin. Chang. Res.* **2011**, *7*, 197–203. (In Chinese)
58. CO_2 Emissions from Fuel Combustion Highlights. 2017. Available online: https://www.iea.org/publications/freepublications/publication/CO2EmissionsfromFuelCombustionHighlights2017.pdf (accessed on 9 August 2018).